Acta Crystallographica Section B
Structural Science
ISSN 0108-7681

Molecular and crystal properties of ethyl 4,6-dimethyl-2-thioxo-1,2,3,4-tetrahydropyrimidine-5-carboxylate from experimental and theoretical electron densities

V. G. Tsirelson,[a]* A. I. Stash,[b] V. A. Potemkin,[c] A. A. Rykounov,[c] A. D. Shutalev,[d] E. A. Zhurova,[e] V. V. Zhurov,[e] A. A. Pinkerton,[e] G. V. Gurskaya[f] and V. E. Zavodnik[b]

[a]Mendeleev University of Chemical Technology, 9 Miusskaya Square, 125047 Moscow, Russia, [b]Karpov Institute of Physical Chemistry, 10 Vorontsovo Pole, 105064 Moscow, Russia, [c]Chelyabinsk State University, 129 Br. Kashirinych Street, 454021 Chelyabinsk, Russia, [d]Lomonosov State Academy of Fine Chemical Technology, 86 Vernadsky Prospect, 119571 Moscow, Russia, [e] Department of Chemistry, University of Toledo, Toledo, Ohio 43606, USA, and [f]Engelhardt Institute of Molecular Biology, Russian Academy of Sciences, 32 Vavilova Street, 119991 Moscow, Russia

Correspondence e-mail: tsirel@muctr.edu.ru

Received 7 March 2006
Accepted 3 May 2006

The electron density and electronic energy densities in ethyl 4,6-dimethyl-2-thioxo-1,2,3,4-tetrahydropyrimidine-5-carboxylate have been studied from accurate X-ray diffraction measurements at 110 K and theoretical single-molecule and periodic crystal calculations. The Quantum Theory of Atoms in Molecules and Crystals (QTAMC) was applied to analyze the electron-density and electronic energy-density features to estimate their reproducibility in molecules and crystals. It was found that the local electron-density values at the bond critical points derived by different methods are in reasonable agreement, while the Laplacian of the electron density computed from wavefunctions, and electron densities derived from experimental or theoretical structure factors in terms of the Hansen–Coppens multipole model differ significantly. This disagreement results from insufficient flexibility of the multipole model to describe the longitudinal electron-density curvature in the case of shared atomic interactions. This deficiency runs through all the existing QTAMC bonding descriptors which contain the Laplacian term. The integrated atomic characteristics, however, suffer noticeably less from the aforementioned shortcoming. We conclude that the electron-density and electronic energy QTAMC characteristics derived from wavefunctions, especially the integrated quantities, are nowadays the most suitable candidates for analysis of the transferability of atoms and atomic groups in similar compounds.

1. Introduction

All recently undertaken studies of the electron density in peptides, biomolecules and related compounds eventually face the question 'how transferable are the characteristics of the electron density in a series of similar compounds as well as among different conformers of the same molecule?'. Some workers suggest using the multipole-model parameters as the transferable moieties (Pichon-Pesme *et al.*, 1995; Jelsch *et al.*, 2000; Pichon-Pesme *et al.*, 2004; Koritsanszky *et al.*, 2002; Volkov, Koritsanszky, Li & Coppens, 2004; Volkov, Li, Koritsanszky & Coppens, 2004; Lecomte *et al.*, 2005), while others (Chang & Bader, 1992; Popelier & Bader, 1994; Breneman & Rhem, 1997; Popelier, 1999; O'Brien & Popelier, 1999, 2001; Matta & Bader, 2000, 2002, 2003; Dittrich *et al.*, 2002; Whitehead *et al.*, 2003; Popelier & Aicken, 2003; Dittrich *et al.*, 2003; Cortes-Guzman & Bader, 2004) deal with characteristics arising from Bader's (1990, 2005) Quantum Theory of Atoms in Molecules and Crystals (QTAMC). The question of whether experimental or theoretical electron densities provide the most reliable basis for such an analysis is also the subject of some discussion (Pichon-Pesme *et al.*, 2004; Volkov, Korit-

sanszky, Li & Coppens, 2004). Unfortunately, no definitive answer to this question has been provided until now.

Recently, we initiated a study of the conformation-transferable electron-density and electronic-energy QTAMC properties of functionally substituted hydropyrimidines to establish a correlation between their conformation-dependent electronic features and their biological activity. We have considered some of the esters of 2-oxo-(or thioxo-)1,2,3,4-tetrahydropyrimidine-5-carboxylic acids (Fig. 1), the Biginelli (1893) compounds. The latter have attracted considerable interest in recent years (Kappe, 1993, 2000*a*,*b*; Shutalev & Kuksa, 1997) owing to their multifaceted pharmacological profiles: they have emerged as orally active antihypertensive agents (Atwal *et al.*, 1991; Grover *et al.*, 1995), mitotic kinesin Eg5 inhibitors (Haggarty *et al.*, 2000), α_{1a} adrenergic-receptor-selective antagonists (Nagarathnam *et al.*, 1999) *etc*. The studies of the structure of Biginelli compounds by computational, X-ray diffraction and NMR methods were undertaken (Rovnyak *et al.*, 1995; Shishkin *et al.*, 1997; Kappe *et al.*, 1997, 2000; Fabian *et al.*, 1998; Uray *et al.*, 2001; Gurskaya *et al.*, 2003*a*,*b*) with a special interest in the correlation between the stereochemistry of the pyrimidine ring and the biological activity of these compounds.

This work reports the results of a joint accurate low-temperature X-ray diffraction and non-empirical quantum-chemical study of bonding in ethyl 4,6-dimethyl-2-thioxo-1,2,3,4-tetrahydropyrimidine-5-carboxylate (1). We aim to elucidate which of the topological electron-density and electronic energy-density features are reproducible in the molecules and crystals. However, in this work we restrict ourselves to the topological characteristics of a conformer of (1), the geometry of which is close to the experimental one. The analysis of the transferable/nontransferable features of the whole set of conformers of (1) is presented elsewhere (Rykounov *et al.*, 2005).

2. Experimental

Compound (1) was prepared according to the general method of synthesis of the Biginelli compounds, which was developed recently and is shown in (I) (Shutalev & Kuksa, 1997; Shutalev *et al.*, 1998). *N*-(1-Tosylethyl)thiourea (2), which is required for the synthesis of (1), was obtained in 97% yield by the three-component condensation of thiourea, acetaldehyde and *p*-toluenesulfinic acid in water at room temperature for 22.5 h [see (I)]. Reaction of (2) with the potassium enolate of ethyl acetoacetate (ethanol, room temperature, 20.5 h), generated by the treatment of the corresponding CH-acid (3) with potassium hydroxide in ethanol, gave ethyl 4-hydroxy-4,6-dimethyl-2-thioxohexahydropyrimidine-5-carboxylate (4). The latter, without isolation, was dehydrated into ethyl 4,6-dimethyl-2-thioxo-1,2,3,4-tetrahydropyrimidine-5-carboxylate (1) in 78% overall yield after the addition of *p*-toluenesulfonic acid to the reaction mixture, followed by refluxing over 1.5 h. Other details of the synthesis as well as the spectroscopic characterization of (1) have been deposited.[1]

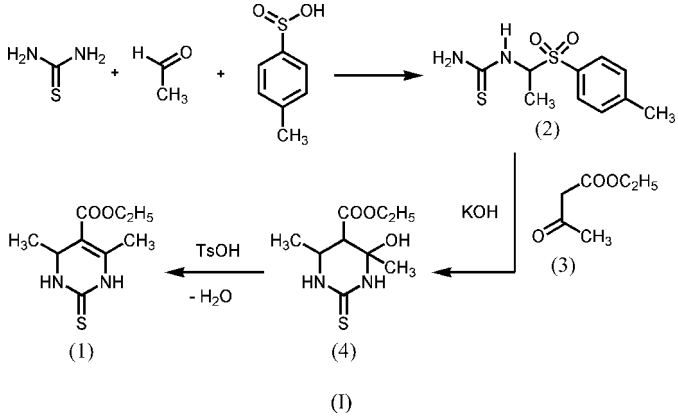

(I)

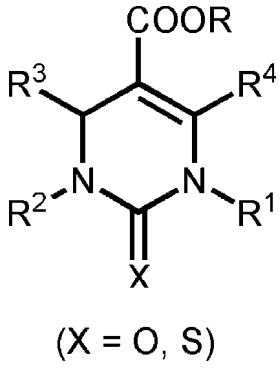

(X = O, S)

Figure 1
General structure formula of the Biginelli compounds.

2.1. Data collection and reduction

Crystals suitable for accurate X-ray structure analysis were prepared by the slow evaporation of a saturated solution of (1) in ethanol. A colorless crystal specimen was mounted on a 0.1 mm capillary and cooled down to 110 K with an Oxford Cryostream cooling device. The X-ray diffraction experiment was performed using a Bruker platform diffractometer with a SMART 6000CCD detector. ω scans with a 0.3° step were performed at a detector distance of 5.24 cm. Two detector settings of $2\theta = -15$ and $-75°$, and several different φ settings were used. Owing to the severe 'bleeding' of the strongest reflections, the low-angle data were measured twice with 15 and 45 s exposure times. The 'bleeding' reflections were then removed from the 45 s data subset and the two subsets were scaled together. For the high-angle data an exposure time of 150 s was used. The first 100 frames were repeated at the end of each detector setting measurement: no X-ray intensity decay was found.

Data integration and unit-cell refinement were performed with the program *SAINT* (Siemens, 1996*b*). An empirically chosen integration box size of 1.0 × 1.0 × 0.6° for the low-angle data and 1.8 × 1.8 × 1.1° box size for the high-angle

[1] Supplementary data for this paper are available from the IUCr electronic archives (Reference: AV5058). Services for accessing these data are described at the back of the journal.

Table 1
Experimental details.

Crystal data	
Chemical formula	$C_9H_{14}N_2O_2S$
M_r	214.28
Cell setting, space group	Triclinic, $P\bar{1}$
Temperature (K)	110.0 (1)
a, b, c (Å)	7.2934 (2), 7.8145 (2), 10.2181 (3)
α, β, γ (°)	87.055 (1), 70.569 (1), 72.898 (1)
V (Å^3)	524.22 (3)
Z	2
D_x (Mg m^{-3})	1.358
Radiation type	Mo $K\alpha$
No. of reflections for cell parameters	71 444
θ range (°)	2.1–55.8
μ (mm^{-1})	0.29
Crystal form, color	Rhombic, colorless
Crystal size (mm)	0.36 × 0.24 × 0.16
Data collection	
Diffractometer	Bruker diffractometer with a SMART 6000CCD detector
Data collection method	ω scan
Absorption correction	None
No. of measured, independent and observed reflections	71 444, 12 501, 9412
Criterion for observed reflections	$I > 3\sigma$
R_{int}	0.029
θ_{max} (°)	55.8
Range of h, k, l	$0 \Rightarrow h \Rightarrow 16$ $-16 \Rightarrow k \Rightarrow 18$ $-22 \Rightarrow l \Rightarrow 23$
Refinement	
Refinement on	F^2
$R[F^2 > 2\sigma(F^2)]$, $wR(F^2)$, S	0.019, 0.022, 1.20
No. of reflections	9412
No. of parameters	398
H-atom treatment	Refined independently
Weighting scheme	$w = 1/[\sigma^2(F^2)]$
$(\Delta/\sigma)_{max}$	0.020
$\Delta\rho_{max}$, $\Delta\rho_{min}$ (e Å^{-3})	0.13, −0.22

Computer programs used: *SORTAV* (Blessing, 1987, 1989), *SMART* (Siemens, 1996*a*), *SAINT* (Siemens, 1996*b*), *SHELXTL* (Sheldrick, 1997), *MOLDOS*2004 (Stash, 2003), *WinXPRO* (Stash & Tsirelson, 2002, 2005).

data, and the profile fitting procedure based on strong ($I > 20\sigma$) reflections allowed us to obtain the best internal consistency ($R_{int} = 0.029$). The data were averaged (scaled and merged) with the program *SORTAV* (Blessing, 1987, 1989). No absorption correction was applied ($\mu = 0.29$ mm^{-1}). Crystallographic data for (1) are presented in Table 1. A view of the crystal packing and hydrogen-bond pattern in (1) is given in Fig. 2.

2.2. Refinements

The structure of (1) was first refined by full-matrix least-squares using the spherical-atom model. The room-temperature structural parameters of Zavodnik *et al.* (2005) were used as initial values. The atomic relativistic scattering factors and anomalous scattering corrections were taken from the *International Tables for Crystallography* (1995). The atomic displacements were modeled in the anisotropic harmonic approximation. No extinction was found for the crystal. The resulting refinement indices were $R = 0.0255$, $wR = 0.0808$ and $S = 1.098$.

The Hansen & Coppens (1978) multipole structural model was used in a subsequent refinement. The atomic many-configuration relativistic wavefunctions from Macchi & Coppens (2001) were used to describe both core and valence densities. The multipole functions were modeled up to octupoles for C, N, O and S atoms (the inclusion of hexadecupoles did not change the electron density meaningfully) and up to dipoles for H atoms.

Refinements based on $|F|$ with least-squares weights equal to $1/[\sigma^2(F) + 0.00005F^2]$ were carried out with *MOLDOS*2004 (Stash, 2003) – a modified version of the programs *MOLLY* (Hansen & Coppens, 1978) and *MOLDOS*97 (Protas, 1997). First, the positional parameters and anisotropic atomic displacement parameters of the non-H atoms were refined in the high-angle region ($\sin\theta/\lambda > 0.65$ Å^{-1}). The C—H and N—

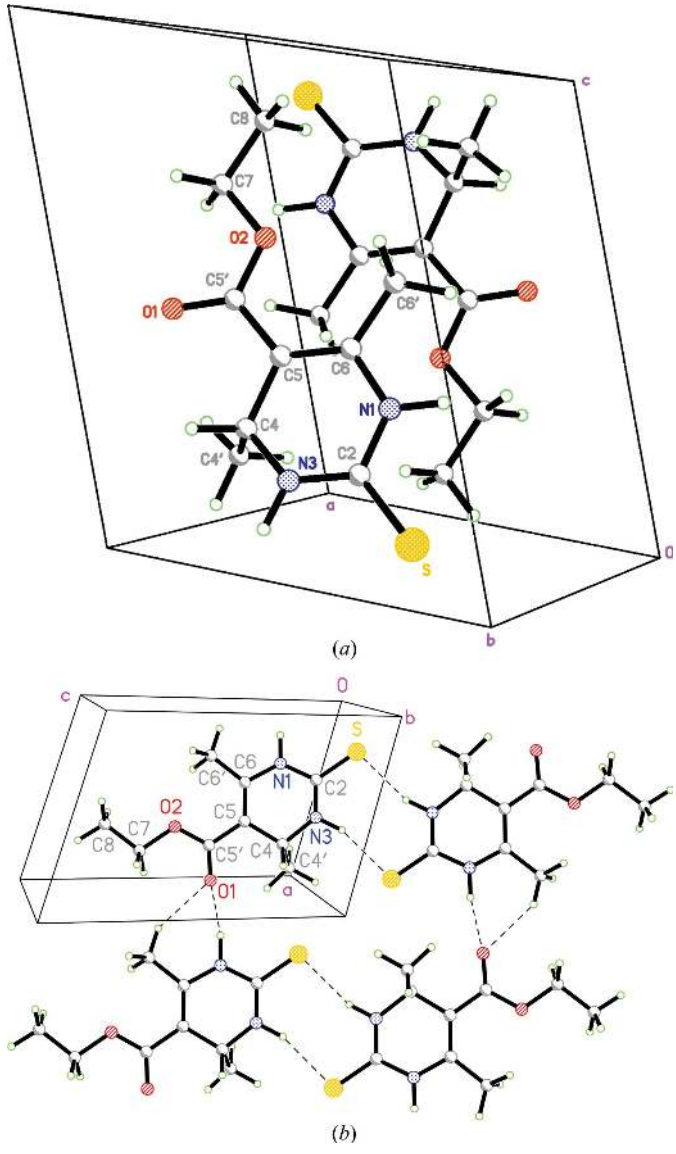

Figure 2
A view of (*a*) the crystal packing and (*b*) the hydrogen-bond pattern in (1).

Table 2
Characteristics of the intramolecular bond critical points.

Experimental results are given in the first line, multipole-modeled results from the DFT/B3LYP 6-31G** structure factors for a crystal at the experimental geometry are listed in the second line, and theoretical results for a single molecule at the experimental geometry are presented in the third line [DFT/B3LYP 6-311G(d,p), the virial ratio $V/G = 2.0033$] and the fourth line [HF/6-311G(d,p), the virial ratio $V/G = 2.0001$]. See text for details.

Bond	R (Å)	$\rho(\mathbf{r})$ (e Å^{-3})	$\nabla^2\rho$ (e Å^{-5})	$g_b(\mathbf{r})$ (a.u.)	v_b (a.u.)	$h_{e,b}(\mathbf{r})$ (a.u.)
S—C2	1.689	1.425 (18)	−2.73 (19)	0.196	−0.421	−0.225
		1.357	−4.94	0.164	−0.379	−0.215
		1.406	−2.49	0.216	−0.458	−0.242
		1.399	−2.30	0.222	−0.440	−0.218
O1—C5′	1.225	3.041 (45)	−40.67 (161)	0.479	−1.380	−0.901
		2.757	−21.19	0.499	−1.219	−0.719
		2.739	−9.13	0.589	−1.272	−0.683
		2.799	−8.50	0.571	−1.288	−0.717
O2—C5′	1.334	2.256 (39)	−25.37 (119)	0.287	−0.837	−0.550
		2.107	−19.84	0.275	−0.756	−0.481
		2.072	−10.72	0.338	−0.786	−0.449
		2.084	−9.83	0.320	−0.804	−0.484
O2—C7	1.451	1.647 (35)	−7.21 (72)	0.224	−0.522	−0.299
		1.524	−3.55	0.216	−0.469	−0.253
		1.546	−7.27	0.210	−0.496	−0.286
		1.484	−7.05	0.190	−0.466	−0.276
N1—C2	1.369	2.27 (37)	−21.98 (81)	0.316	−0.861	−0.544
		2.123	−19.56	0.282	−0.768	−0.485
		2.125	−22.11	0.198	−0.626	−0.428
		2.305	−20.47	0.191	−0.579	−0.387
N1—C6	1.391	2.101 (38)	−17.05 (75)	0.293	−0.762	−0.470
		1.994	−15.35	0.270	−0.700	−0.430
		2.013	−19.73	0.189	−0.583	−0.394
		2.209	−19.52	0.198	−0.566	−0.367
N1—H1	1.010	2.190 (18)	−29.78 (23)	0.234	−0.777	−0.543
		2.192	−28.76	0.242	−0.782	−0.540
		2.301	−41.66	0.049	−0.531	−0.481
		2.443	−45.28	0.044	−0.495	−0.488
N3—C2	1.328	2.475 (40)	−25.63 (87)	0.362	−0.990	−0.628
		2.330	−24.42	0.319	−0.891	−0.572
		2.300	−23.17	0.252	−0.744	−0.492
		2.466	−23.62	0.243	−0.730	−0.487
N3—C4	1.468	1.703 (35)	−9.12 (55)	0.226	−0.547	−0.321
		1.671	−8.13	0.224	−0.533	−0.308
		1.706	−15.36	0.129	−0.418	−0.289
		1.567	−14.00	0.117	−0.387	−0.270
N3—H3	1.009	2.256 (21)	−28.84 (26)	0.263	−0.825	−0.562
		2.187	−27.45	0.249	−0.783	−0.534
		2.295	−40.53	0.051	−0.522	−0.471
		2.175	−41.66	0.054	−0.552	−0.497
C4—C4′	1.532	1.62 (28)	−8.97 (6)	0.206	−0.505	−0.299
		1.541	−7.95	0.190	−0.463	−0.273
		1.638	−13.22	0.056	−0.250	−0.194
		1.575	−12.91	0.052	−0.249	−0.197
C4—C5	1.515	1.703 (31)	−10.08 (9)	0.220	−0.544	−0.324
		1.627	−9.45	0.203	−0.504	−0.301
		1.748	−14.23	0.058	−0.263	−0.205
		1.669	−13.00	0.058	−0.247	−0.189
C4—H4	1.093	1.835 (24)	−16.53 (14)	0.214	−0.599	−0.385
		1.850	−16.21	0.221	−0.388	−0.608
		1.976	−24.90	0.039	−0.336	−0.297
		2.149	−24.20	0.035	−0.324	−0.288
C4′—H41′	1.058	1.751 (24)	−14.46 (19)	0.203	−0.556	−0.353
		1.920	−17.61	0.231	−0.645	−0.414
		1.986	−25.15	0.049	−0.358	−0.310
		1.994	−23.91	0.052	−0.363	−0.311
C4′—H42′	1.058	1.751 (24)	−14.81 (19)	0.201	−0.555	−0.354
		1.914	−17.42	0.231	−0.643	−0.412
		1.973	−24.79	0.052	−0.362	−0.309
		1.954	−25.79	0.053	−0.338	−0.285
C4′—H43′	1.058	1.730 (24)	−13.76 (19)	0.202	−0.547	−0.345
		1.898	−17.07	0.229	−0.635	−0.406
		1.976	−24.85	0.050	−0.359	−0.309
		1.962	−25.72	0.054	−0.356	−0.302

H bond distances were elongated up to their standard recommended values (*International Tables for Crystallography*, 1995) in order to describe them more accurately. The isotropic atomic displacement parameters of the H atoms were refined in the low-angle region ($\sin\theta/\lambda < 0.65$ Å^{-1}). The atomic positional and displacement parameters obtained in this refinement have been deposited.

The multipole parameter refinement was carried out in the range $0.0 < \sin\theta/\lambda < 1.16$ Å^{-1} and converged to $R = 0.0194$, $wR = 0.0221$ and $S = 1.20$ for 9412 unique reflections with $|F| > 3\sigma(|F|)$. The residual Fourier map (deposited) showed an average electron-density noise of 0.04 e Å^{-3}. Thus, the experimental electron density of (1) was adequately described by the multipole model.

The multipole parameters obtained were used to reconstruct the electron density in (1), which appeared to be positive everywhere. Calculated characteristics of the bond critical points in the electron density are listed in Tables 2 and 3. The network of the bond paths superimposed on the Laplacian of the total electron density in a selected plane of (1) is presented in Fig. 3(*a*). Maps of errors in $\rho(r)$ and $\nabla^2\rho(r)$ were estimated according to Lobanov *et al.* (1990) and deposited. All the calculations were performed with the latest version of the program *WinXPRO* (Stash & Tsirelson, 2002, 2005).

2.3. Theoretical calculations

Quantum-chemical computations of molecule (1), as well as molecular dimers simulating the hydrogen-bond system in the crystal, were performed with the program *PC*, *GAMESS* version (Granovsky, 2003) of the *GAMESS*(US) package (Schmidt *et al.*, 1993), for the experimental geometry and for geometries optimized at the HF/6-311G(d,p) and DFT B3LYP/6-311G(d,p) levels of theory. Structure optimization of the molecule was carried out starting from the X-ray structural parameters, followed by a harmonic vibration frequency calculation which confirmed that a stable minimum energy conformer had been obtained. Then, the complete *ab initio* DFT B3LYP/6-311G(d,p) conformation analysis of (1) was performed in the energy range of 40.8 kJ mol^{-1} relative to the conformer corresponding to the experimental conformation. The many-electron wavefunctions obtained were used to compute the electron density and the critical point features for each conformation. Later in this work, we will focus on the characteristics of the conformer corresponding to the experimental geometry (Table 2); the features of the whole set

Table 2 (continued)

Bond	R (Å)	$\rho(\mathbf{r})$ (e Å^{-3})	$\nabla^2\rho$ (e Å^{-5})	$g_b(\mathbf{r})$ (a.u.)	v_b (a.u.)	$h_{e,b}(\mathbf{r})$ (a.u.)
C5—C5′	1.466	1.912 (33)	−14.07 (20)	0.254	−0.653	−0.400
		1.828	−13.68	0.231	−0.604	−0.373
		1.852	−16.83	0.072	−0.319	−0.247
		1.930	−18.08	0.066	−0.297	−0.231
C5—C6	1.361	2.262 (39)	−19.39 (40)	0.330	−0.862	−0.531
		2.222	−19.71	0.314	−0.833	−0.519
		2.192	−21.82	0.128	−0.319	−0.354
		2.329	−23.03	0.130	−0.509	−0.379
C6—C6′	1.499	1.762 (29)	−11.48 (11)	0.227	−0.573	−0.346
		1.649	−10.05	0.205	−0.514	−0.309
		1.721	−14.94	0.062	−0.280	−0.217
		1.820	−15.71	0.066	−0.287	−0.221
C6′—H61′	1.058	1.845 (29)	−12.74 (47)	0.243	−0.618	−0.375
		1.890	−16.92	0.227	−0.630	−0.403
		1.973	−24.84	0.049	−0.355	−0.306
		2.078	−24.92	0.046	−0.358	−0.312
C6′—H62′	1.058	1.869 (30)	−14.86 (40)	0.235	−0.624	−0.389
		1.910	−17.34	0.230	−0.640	−0.410
		1.976	−24.81	0.052	−0.361	−0.309
		1.957	−23.32	0.056	−0.350	−0.293
C6′—H63′	1.058	1.823 (29)	−13.86 (43)	0.228	−0.601	−0.372
		1.902	−16.86	0.231	−0.637	−0.406
		1.988	−25.12	0.048	−0.358	−0.309
		2.112	−23.44	0.051	−0.391	−0.339
C7—C8	1.509	1.723 (20)	−11.31 (3)	0.217	−0.551	−0.334
		1.619	−9.36	0.201	−0.499	−0.298
		1.715	−14.85	0.058	−0.270	−0.212
		1.662	−15.47	0.059	−0.276	−0.217
C7—H71	1.092	1.854 (24)	−17.14 (14)	0.215	−0.607	−0.393
		1.832	−16.04	0.216	−0.598	−0.382
		1.931	−23.96	0.036	−0.320	−0.284
		1.892	−22.14	0.035	−0.336	−0.301
C7—H72	1.092	1.808 (24)	−16.00 (16)	0.209	−0.584	−0.375
		1.839	−16.25	0.216	−0.601	−0.385
		1.924	−23.81	0.036	−0.318	−0.283
		2.110	−23.17	0.036	−0.307	−0.270
C8—H81	1.058	1.849 (0)	−15.70 (1)	0.223	−0.610	−0.386
		1.914	−17.60	0.230	−0.642	−0.413
		1.972	−24.74	0.051	−0.358	−0.308
		2.154	−24.22	0.052	−0.346	−0.294
C8—H82	1.058	1.766 (0)	−14.58 (1)	0.207	−0.565	−0.358
		1.908	−17.08	0.231	−0.640	−0.409
		1.978	−24.87	0.051	−0.361	−0.309
		2.132	−25.81	0.050	−0.378	−0.328
C8—H83	1.057	1.738 (0)	−13.85 (1)	0.204	−0.551	−0.347
		1.902	−17.09	0.230	−0.637	−0.407
		1.974	−24.83	0.051	−0.360	−0.309
		1.991	−24.58	0.055	−0.392	−0.337
O2···C6′	2.757	0.116 (1)	1.68 (5)	0.015	−0.012	0.003
		0.106	1.62	0.014	−0.011	0.003
		0.103	1.52	0.013	−0.011	0.002
		0.108	1.57	0.013	−0.010	0.002

of conformers will be described elsewhere (Rykounov *et al.*, 2005). The Laplacian of the electron density was also calculated (Fig. 3*b*). All the molecular QTAMC functions and characteristics were determined using a locally modified version of AIMPAC (Biegler-Konig *et al.*, 1982).

We have also performed calculations on the three-dimensional crystal of (1) at the experimental geometry with the DFT/B3LYP 6-31G** method using the computer program *CRYSTAL*98 (Saunders *et al.*, 1998). The structure factors were computed and the same multipole model (model/*CRYSTAL*98) as that used for the experimental data has been fitted to them. The characteristics of the bond-critical points in the electron density found with this model are listed in Tables 2 and 3.

2.4. Integrated atomic characteristics

The integrated values of the atomic electron population (and the related atomic charges) and atomic electronic energies, H_e, were computed for both experimental and theoretical [both *CRYSTAL*98 and single-molecule DFT B3LYP/6-311G(d,p)] data (Table 4). During the calculations, the value of the integral $\nabla^2\rho(\mathbf{r})\mathrm{d}V$ was checked and was shown to be less than $\pm 0.5 \times 10^{-3}$ a.u.

3. Results and discussion

3.1. Molecular and crystal structure

The structure of (1) (Fig. 2) consists of a heterocyclic tetrahydropyrimidine ring with an ethoxycarbonyl group and two methyl substituents. The C2, N3, C5 and C6 atoms of the ring are in the same plane, while the N1 and C4 atoms deviate from the C2—N3—C5—C6 plane by 0.09 and 0.27 Å, respectively, generating a distorted boat conformation. The C5 and C6 atoms, and the carboxyl group represent a planar conjugated system. The C7 and C8 atoms of the ethyl group deviate from the plane by 0.06 and 0.02 Å, respectively. The C4 atom is a chiral centre. The intermolecular N3—H3···S^{ii} hydrogen bonds link molecules of (1) in the crystal through a center of symmetry forming dimers, the latter being linked by bifurcated intermolecular C6′—H62′···O1^{i} and N1—H1···O1^{i} hydrogen bonds to form a two-dimensional network alternately consisting of the *R* and *S* isomers. Geometrical parameters of the hydrogen bonds are given in Table 3.

3.2. Electron-density and energy-density critical-point analysis

QTAMC (Bader, 1990) allows us to identify a network of atomic interaction lines, and the regions of local electron-density concentration and depletion associated with bond formation. This theory also provides a simple classification scheme for atomic interactions in terms of the electron density, $\rho(\mathbf{r})$, its gradient field, $\nabla\rho(\mathbf{r})$, and Laplacian, $\nabla^2\rho(\mathbf{r})$, kinetic energy density, $g(\mathbf{r}) > 0$, potential energy density, $v(\mathbf{r}) < 0$, and the local electronic energy density, $h_e(\mathbf{r}) = g(\mathbf{r}) + v(\mathbf{r})$. In the first approximation, considering these functions at the bond-critical points (CPs), it is possible to discern three main types of atomic interactions. According to Cremer & Kraka (1984), Macchi *et al.* (1998), Tsirelson (1999), Bianchi *et al.* (2000), Espinosa *et al.* (2002), Macchi & Sironi (2003), Marabello *et al.* (2004), Gatti (2005) and Stash *et al.* (2005), closed-shell atomic interactions are characterized by $\rho_b < 0.3$ e Å^{-3}, $\nabla^2\rho_b > 0$, $|\lambda_1|/\lambda_3 < 0.25$, $h_{e,b} > 0$, and $g_b/\rho_b > 1$; shared interactions exhibit ρ_b

Table 3
Geometrical and topological parameters for the hydrogen bonds.

Experimental results are given in the first line, multipole-modeled results from the DFT/B3LYP 6-31G** structure factors for a crystal at the experimental geometry are listed in the second line, theoretical results for the dimers at the experimental geometry (DFT/B3LYP 6-311G(d,p) are presented in the third line.

D—H···A	$r(D\cdots A)$ (Å)	$r(H\cdots A)$ (Å)	$a(D$—H···$A)$ (grad)	ρ_b (e Å^{-3})	$\nabla^2\rho_b$ (e Å^{-5})	g_b (a.u.)	v_b (a.u.)	$h_{e,b}$ (a.u.)
N1—H1···O1^{i}	2.95	1.95	169.2	0.105 (3)	2.31 (3)	0.0188	−0.0136	0.0052
				0.125	2.37	0.0201	−0.0156	0.0045
				0.143	0.56	0.0198	−0.0161	0.0036
N3—H3···S^{ii}	3.34	2.37	160.9	0.098 (4)	1.30 (3)	0.0115	−0.0095	0.0020
				0.116	1.48	0.0135	−0.0117	0.0020
				0.148	0.29	0.0118	−0.0117	0.0002
C6′—H62′···O1^{i}	3.35	2.40	148.3	0.056 (3)	0.87 (1)	0.0070	−0.0050	0.0020
				0.062	0.92	0.0075	−0.0055	0.0020
				0.075	0.22	0.0079	−0.0068	0.0011

Symmetry codes: (i) $x-1, y, z$; (ii) $1-x, 2-y, -z$.

> 1.0 e Å^{-3}, $\nabla^2\rho_b < 0$, $|\lambda_1|/\lambda_3 > 1$, $h_{e,b} < 0$, and $g_b/\rho_b < 1$ and intermediate interactions show $0.3 < \rho_b < 1.0$ e Å^{-3}, $\nabla^2\rho_b > 0$, $|\lambda_1|/\lambda_3 > 0.20$, $h_{e,b} < 0$, and $g_b/\rho_b > 1$ (λ_1 is the most negative electron-density curvature in the direction perpendicular to the internuclear line, while $\lambda_3 > 0$ is the electron-density curvature along this line). This quantitative bond characterization is directly applicable to both the theoretical and experimental electron density. In the latter case, the function $g(\mathbf{r})$ is typically approximated by the Kirzhnits (1957) or Lee *et al.* (1991) formulae of density-functional theory (Abramov, 1997; Espinosa *et al.*, 1998; Tsirelson, 2002, 2003), while the potential energy density, $v(\mathbf{r})$, is calculated according to Espinosa *et al.* (1998) using a local form of the virial theorem (Bader & Beddall, 1972).

Our general aim is to determine which of the electron-density and electronic energy-density characteristics of QTAMC are the most suitable for analysis of the transferability of atoms and atomic groups in similar compounds. To put the discussion on a firm basis, in this work we aim to elucidate how reproducible the ED (electron density) features employed in such an analysis are. At this point, we must keep in mind that the experimental and periodic crystal theoretical (*CRYSTAL*98 type) densities imply all the intra- and intermolecular interactions, while single-molecule calculations do not. In addition, reproducibility of the single-molecule ED derived by different theoretical methods depends on the level and type of the calculations (Flaig *et al.*, 2002).

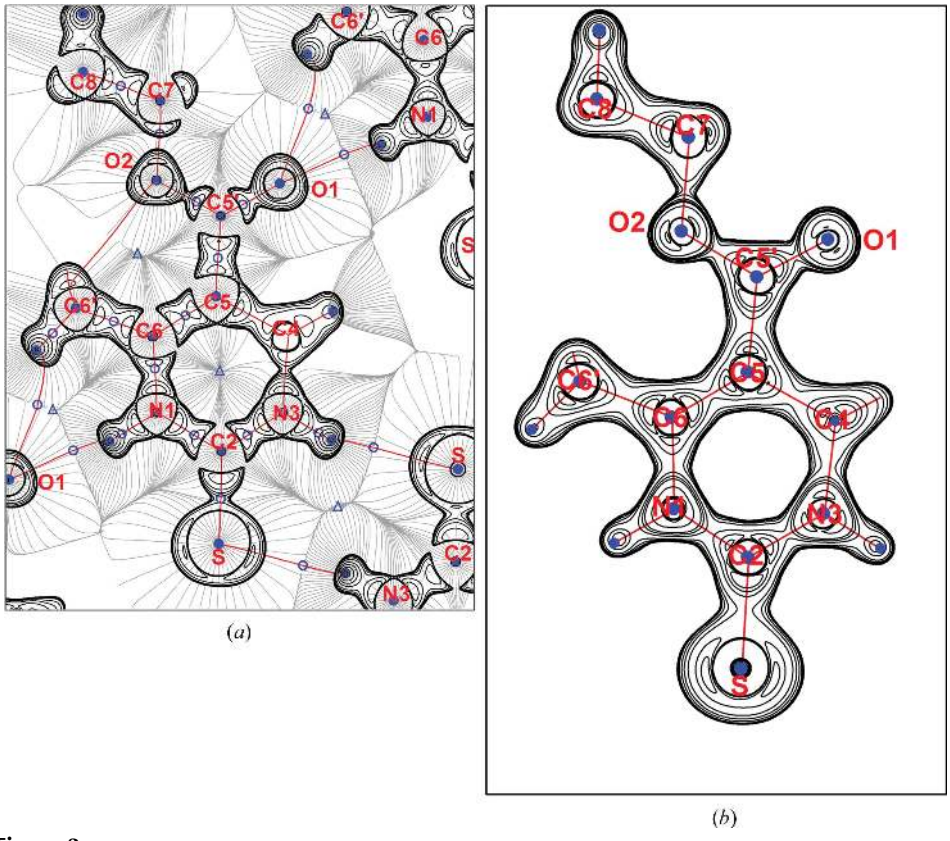

Figure 3
Laplacian of the electron density in (1) (the plane passes through the N1, N3 and O2 atoms): (*a*) the map modeled with the multipole experimental parameters for a crystal and superimposed with the gradient field $\nabla\rho(\mathbf{r})$. The bond CPs are shown as open circles, while the ring critical points are denoted as triangles. (*b*) The map computed using single-molecule DFT B3LYP/6-311G(d,p) wavefunctions. Only charge-concentration areas are shown; the line intervals are $(2, 4, 8) \times 10^n$ e Å^{-5} ($-2 \le n \le 2$).

Table 2 shows that all regular intramolecular atomic interactions in (1) belong to shared interactions (or covalent bonds), as expected. Comparison of the experimental (model), theoretical (model/*CRYSTAL*98) and theoretical single-molecule (wavefunction) electron-density and energy-density characteristics at the intramolecular bond-critical points (CPs) of (1) (Table 2) reveals that values of ρ_b depend only slightly on their derivation method. Model/experimental and model/*CRYSTAL*98 Laplacian values are

Table 4
Atomic volumes (Ω), charges (Q) and electronic energies (H) integrated within the atomic basins.

Experimental values are given in the first line, and theoretical values obtained from the multipole-modeled *CRYSTAL*98 structure factors and DFT B3LYP/6-311G(d,p) single-molecule calculations (both computed at the experimental geometry) are listed in the second and third lines, respectively.

Atom	Ω (Å^3)	Q (e)	$-H$ (a.u.)
S	33.776	0.01	400.914
	37.150	0.00	399.782
	37.982	0.00	397.041
O1	16.187	−1.17	76.135
	16.542	−1.17	75.737
	19.055	−1.14	75.584
O2	13.642	−1.13	76.140
	13.658	−1.02	75.619
	13.884	−1.08	75.623
N1	13.655	−1.12	55.905
	13.950	−1.07	55.661
	14.001	−1.14	55.183
N3	13.051	−1.10	55.909
	13.111	−1.05	55.653
	13.647	−1.12	55.171
C2	7.411	0.68	37.909
	7.202	0.67	37.844
	8.276	0.67	37.444
C4	6.748	0.28	38.208
	6.886	0.22	38.222
	6.642	0.39	37.654
C4′	12.099	−0.21	38.688
	10.750	−0.07	38.571
	9.670	0.07	37.902
C5	9.824	−0.13	38.663
	10.045	−0.08	38.481
	11.229	−0.09	39.758
C5′	5.984	1.27	37.455
	5.435	1.47	37.157
	5.963	1.47	36.987
C6	8.925	0.24	38.300
	8.695	0.32	38.139
	9.121	0.36	41.945
C6′	11.024	0.08	38.337
	10.905	−0.08	38.571
	11.117	0.08	38.201
C7	8.303	0.23	38.293
	7.899	0.29	38.171
	7.908	0.45	37.595
C8	11.066	0.05	38.375
	10.934	−0.06	38.572
	9.741	0.09	37.886
H1	2.935	0.49	0.334
	2.907	0.47	0.353
	4.307	0.42	0.455
H3	3.308	0.43	0.377
	3.133	0.43	0.369
	4.498	0.41	0.461
H4	6.871	0.10	0.563
	6.461	0.09	0.588
	6.520	0.04	0.629
H41′	6.630	0.15	0.510
	6.784	0.06	0.624
	6.844	0.01	0.633
H42′	8.506	0.15	0.512
	7.862	0.05	0.630
	7.368	−0.02	0.647
H43′	7.997	0.16	0.504
	8.284	0.05	0.641
	7.396	−0.01	0.643
H61′	7.207	0.04	0.656
	7.136	0.07	0.611
	6.914	0.03	0.624
H62′	5.765	0.01	0.676
	5.807	0.06	0.622
	7.083	−0.01	0.645
H63′	5.794	0.04	0.649
	5.960	0.07	0.617
	6.457	0.04	0.627
H71	5.865	0.11	0.553
	5.793	0.06	0.607
	6.824	0.04	0.616
H72	6.191	0.12	0.548
	6.311	0.07	0.607
	6.940	0.04	0.617
H81	8.120	0.07	0.585
	7.725	0.05	0.626
	7.315	−0.01	0.641
H82	6.560	0.06	0.583
	6.444	0.04	0.633
	7.356	−0.01	0.644
H83	8.045	0.07	0.579
	7.577	0.06	0.622
	7.284	−0.01	0.639
Σ	261.489	−0.02	1016.860
	261.346	−0.01	1014.322
	271.342	−0.03	1012.497

close to each other, however, they strongly differ from the single-molecule data; at the same time, $\nabla^2\rho_b$ values for a single molecule computed by the Hartree–Fock and DFT methods are in good agreement. The same picture is observed for energy densities derived by different methods. All these findings completely agree with those of Flaig *et al.* (2002) resulting from a similar consideration of the bond CPs in six amino acids.

The r.m.s. deviations of experimental and DFT/B3LYP 6-311G(d,p) values of the electron density and the Laplacian of the electron density for a single molecule of (1) at the experimental geometry averaged over all intramolecular bond CPs are 0.15 e Å^{-3} and 10 e Å^{-5}, respectively. That is a typical estimate for the discrepancy between the crystalline and single-molecule results. Thus, agreement in the electron density at the covalent bond CPs of (1) can be recognized as quite reasonable, even ignoring crystal effects. At the same time, the Laplacian of the electron density does not exhibit a quantitative agreement.

A significant discrepancy in the model and wavefunction-based Laplacians of the electron density for shared interactions has already been noted in the literature (Bianchi *et al.*, 1996; Spackman *et al.*, 1999; Flaig *et al.*, 2002; Volkov, Li, Koritsanszky & Coppens, 2004; Volkov, Koritsanszky, Li & Coppens, 2004; Coppens & Volkov, 2004; Zhurova *et al.*, 2004; Henn *et al.*, 2004; Hibbs *et al.*, 2005). Insufficient flexibility of existing multipole models to span the charge distribution both close to the nuclei and at the middle-bond area (especially for polar covalent bonds) is considered to be the main reason for this discrepancy (Chandler & Spackman, 1982; Parini *et al.*, 1985; Iversen *et al.*, 1997; de Vries *et al.*, 2000; Volkov *et al.*, 2000; Volkov & Coppens, 2001), the maximum discrepancy being found for the ED curvature along the bond line, λ_3 (Flaig *et al.*, 2002; Volkov *et al.*, 2000). To obtain a quantitative

estimate for these observed discrepancies, we have computed the r.m.s. deviations of the ED curvatures λ_1, λ_2 and λ_3 at the bond CPs in (1) for the different models (Table 5), as well as their ratio to the corresponding average curvature values; the latter yields a relative measure of the spread of the electron-density curvature. Indeed, we found that the λ_3 values clearly show the maximum disagreement. The perpendicular λ_1 and λ_2 ED curvatures are found to be in satisfactory agreement in all of the cases, their spread being roughly described by a normal distribution; the spread in the λ_3 differences is far from a normal distribution (Fig. 4). No correlation was observed for the λ_3 curvatures derived in different ways, excluding the reasonable agreement of the model/experimental and model/*CRYSTAL*98 data. Unfortunately, this agreement is an artifact resulting from using the same multipole model: when the theoretical densities are projected into the multipole density functions through refinement against the theoretical structure factors, the topological properties change and differences between theory and experiment are reduced (Volkov *et al.*, 2000). All our findings for (1) completely agree with the conclusions of similar analyses by Volkov *et al.* (2000) and Flaig *et al.* (2002).

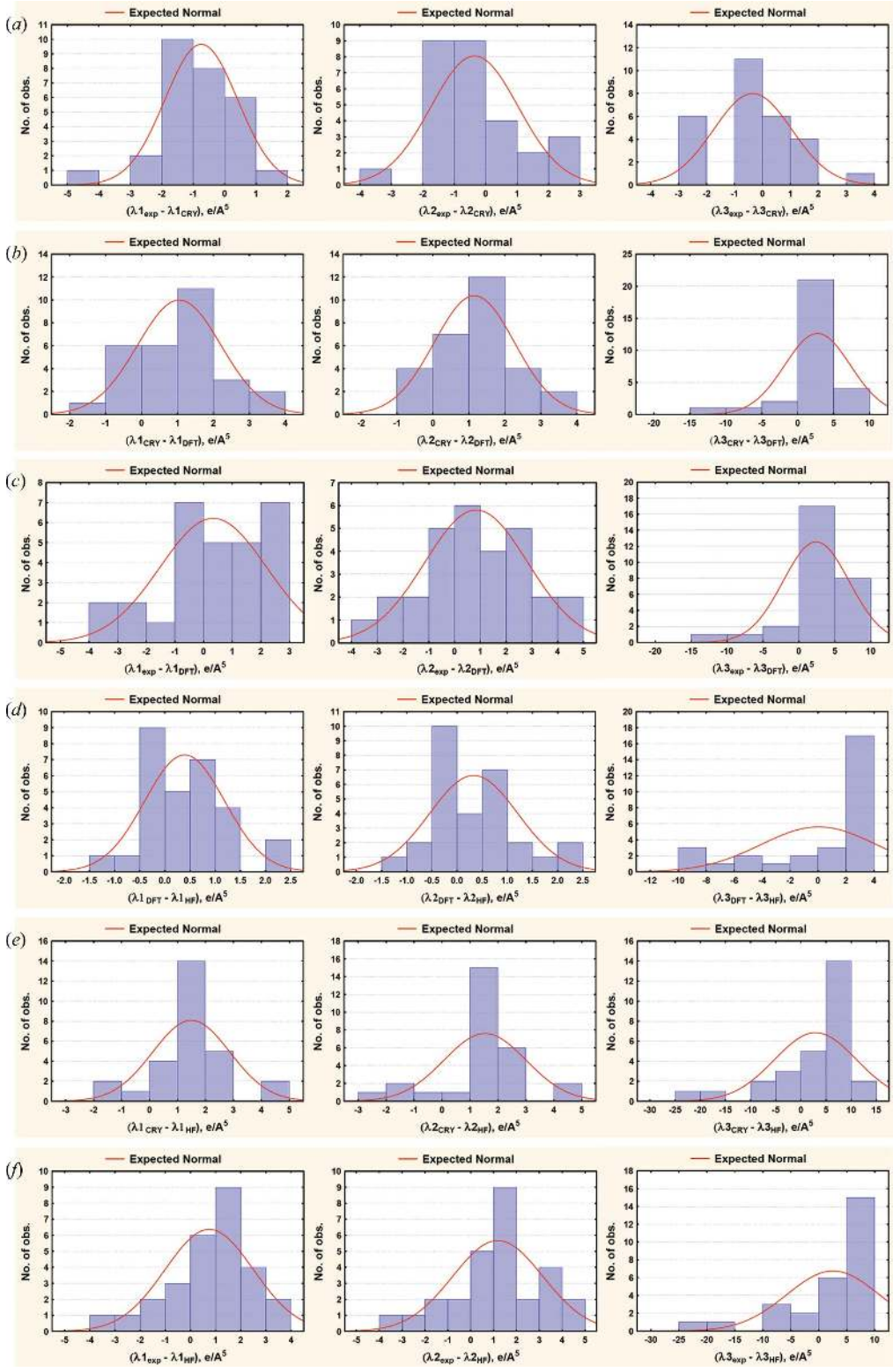

Figure 4
Distribution of the r.m.s. deviations for electron-density curvatures λ_1, λ_2 and λ_3 computed for different combinations of methods: (*a*) model/*CRYSTAL*98 – model/experimental; (*b*) DFT/molecule – model/*CRYSTAL*98; (*c*) DFT/molecule – model/experimental; (*d*) DFT/molecule –HF/molecule; (*e*) HF/molecule – model/*CRYSTAL*98; (*f*) HF/molecule – model/experimental.

It is now clear that comparison of the experimental and theoretical energy-density characteristics for shared interactions should be done with caution. Indeed, the DFT approximate formulae used to compute $g(\mathbf{r})$, $v(\mathbf{r})$ and $h_e(\mathbf{r})$ from the experimental ED contain the Laplacian term, which accounts for the electronic shell structure (Abramov, 1997; Tsirelson, 2002). Apart from the approximate nature of these formulae, the negative Laplacian values for shared inter-

Table 5
The r.m.s. deviations of the electron-density curvatures computed over the intramolecular bond critical points of (1) derived using results of different methods (see text for detail).

Methods	ED curvature	r.m.s (e A^{-5})	r.m.s./$\lambda_{average}$ (%)	Correlation coefficient
DFT_{mol}–HF_{mol}	λ_1	0.79	4.7	0.992
	λ_2	0.87	5.4	0.990
	λ_3	4.12	33.2	0.885
DFT_{mol}–experiment	λ_1	1.86	11.3	0.947
	λ_2	1.99	12.9	0.936
	λ_3	4.61	33.8	0.710
DFT_{mol}–$DFT_{model/CRYSTAL98}$	λ_1	1.16	7.2	0.988
	λ_2	1.12	7.3	0.991
	λ_3	4.58	33.1	0.717
HF_{mol}–experiment	λ_1	1.73	9.7	0.964
	λ_2	1.94	12.4	0.952
	λ_3	8.15	59.9	0.378
HF_{mol}–$DFT_{model/CRYSTAL98}$	λ_1	1.39	8.5	0.989
	λ_2	1.47	9.5	0.986
	λ_3	8.03	58.2	0.409
Experiment–$DFT_{model/CRYSTAL98}$	λ_1	1.15	7.2	0.976
	λ_2	1.38	9.3	0.961
	λ_3	1.38	9.2	0.967

actions are significantly distorted near centers of the internuclear distances because of the multipole model deficiency mentioned above. Thus, as can be seen from Table 2, the energy density at the bond CP for shared interactions lacks, in general, quantitative validity when the analysis is based on the Laplacian-containing formulae. Note, in contrast, that the values of $g(\mathbf{r})$, $v(\mathbf{r})$ and $h_e(\mathbf{r})$ computed with the density-functional formulae at the bond CP for closed-shell and intermediate atomic interactions ($\nabla^2\rho_b > 0$), are in good agreement with the corresponding values derived directly from the Hartree–Fock or Kohn–Sham wavefunctions (Galvez *et al.*, 2001; Farrugia *et al.*, 2003; Tsirelson, 2003). Therefore, this approach is applicable for the description of the local characteristics of closed-shell interactions, in particular, the hydrogen bonds (see below).

Keeping in mind the intrinsic features of the topological analysis based on the Laplacian reconstructed from the multipole model characteristics, as discussed above, we may elaborate on some of the details of the chemical bonding in (1). The formally identical covalent bonds, C2—N1 and C2—N3 or N1—H1 and N3—H3 have slightly different topological characteristics. The difference for the formally single bonds N1—C6 and N3—C4 is even more noticeable: the electron density at the center of the longer N3—C4 bond is more depleted and the Laplacian distribution (Fig. 3) shows some polarity of this bond. Nominally single C—C bonds do not differ much in ρ_b; at the same time, $\nabla^2\rho_b$ values in these bonds do vary significantly. No apparent electron-density equalization at the bond CPs in the C6═C5—C5′═O1 conjugated fragment, which is the most reactive part of (1), was found. The difference in Laplacian distributions between H atoms of the methyl groups at the C4′, C6′ and C8 positions is small, and results from the asymmetry of the intramolecular environment.

A non-standard ('subsidiary') bond CP in the electron density was located between atoms C6′ and O2. The internuclear C6′—O2 distance of 2.757 Å is less than the sum of the van der Waals radii, and is accompanied by a bond CP in the negative potential energy density. Analogous critical points in the promolecule do not exist. Thus, the O2—C5′—C5—C6—C6′ atomic fragment forms a five-membered ring and generates a corresponding ring-critical point (Fig. 3). Note that the topological features of this C6′—O2 bond CP (Table 2) do not allow us to associate it with any of the three types of atomic interactions listed above. Note also that the O2—C6′ bond path is directed to the mid-point of the C6′—H62′ bond and then it is strongly curved towards the C6′ atom. It thus seems that the whole methyl group at the C6' position defines this interaction.

As we reported elsewhere (Rykounov *et al.*, 2005), (1) in the free state shows six stable enantiomer pairs exhibiting the torsion angles $\varphi_{C6-C5-C5'-O1} = 0$ and 180°, and the torsion angles $\varphi_{C5'-O2-C7-C8} = 70$, 180 and 290°. In the solid state, the experiment detects the racemic structure formed by the pair of *R* and *S* enantiomers related through a crystallographic inversion center (Fig. 2*a*). The energy of these conformers in the free state is 0.0006 a.u. higher than the energy of the most energetically stable conformer pair, the latter exhibiting bond CPs, indicating C6′—O2 and C4′—O1 'subsidiary' bonding interactions. In the conformers corresponding to the experimentally observed geometry, the O1 atom is not involved in a direct bonding interaction with the C4′ atom and, therefore, remains open for the formation of the intermolecular hydrogen bond. Such bonds (O1···H1 and O1···H62′) are indeed observed in the crystal (Fig. 2*b* and Fig. 3). The bond-accessible surface of the O1 atom in this conformation calculated according to Connolly (1983, 1985) is 3.10 $Å^2$, whereas the same surface for the conformer pair of minimal energy is 2.10 $Å^2$ (similar values were obtained for all the other conformations). Thus, the hydrogen bonds O1···H1 and O1···H62′ minimize the crystal energy more effectively than the closed-shell interaction C4—O2.

Note that the values of ρ_b and $\nabla^2\rho_b$ of all the covalent bonds in (1) agree quite well with the corresponding values in a number of other experimentally studied molecules of biological interest, for example, L-arginine phosphate monohydrate (Espinosa *et al.*, 1996), DL-histidine (Coppens *et al.*, 1999) and dimethyl-*trans*-2-oxohexahydropyrimidine-4,6-dicarboxylate (Hibbs *et al.*, 2005).

3.3. Atomic charges and atomic energies

The atomic charges and atomic electronic energies calculated by numerical integration over the zero-flux atomic basins Ω_i (Bader, 1990) are listed in Table 4. It should be stressed that the Laplacian term in the DFT energy-density formulae integrates to zero and does not contribute to the atomic energy values. Therefore, the deficiencies in the ED topology features mentioned above manifest themselves only through the error

in $\nabla\rho$, *i.e.* it influences the accuracy of the determination of the atomic volumes and energies to a lesser extent than do errors in $\nabla^2\rho(\mathbf{r})$. Thus, these approximate formulae are applicable to any compound independent of the type of atomic interactions and can provide, in principle, an accuracy of 1% in the energy determination (Politzer & Parr, 1974; Tal & Bader, 1978).

The r.m.s. deviations of single-molecule (DFT B3LYP/6–311**) and experimental values averaged over all the atomic electron population and energies for (1) are 0.11 e (8.2%) and 1.100 a.u. (3.0%), respectively. We conclude that the characteristics derived from integration of the properties over the atomic basins are more reproducible than the corresponding properties at the bond-critical points. We may speculate that the relative invariability of the internal parts of the atomic densities influence the reproducibility of the atomic properties greatly.

Despite the fact that the formally single N1—C6 and N3—C4 bonds exhibit significantly different Laplacian features (see above), the distinction between the integrated characteristics of the N1 and N3 atoms is minimal. The N1 atom has a larger volume than N3, making it more attractive for electrophilic attack. This feature distinguishes (1) from some other hydropyrimidines (Kappe *et al.*, 2000; Hibbs *et al.*, 2005).

Bartashevich *et al.* (2006) have recently found a correlation between the topological properties of the C5 and C6 atoms of the pyrimidine ring and tuberculostatic activity of hydropyrimidines: the tuberculostatic activity is augmented with the increase of the C5 atomic volume and growth of its potential energy, and with the decrease in the potential energy of the C6 atom. The linear relationship $\lg(\mathrm{MIC}) = a + bV_{\mathrm{C5}} - cV_{\mathrm{C6}} + d\Omega_{\mathrm{C5}}$ was obtained for a set of 24 dihydropyrimidine derivatives (MIC is the minimal inhibitory concentration; V is the atomic potential energy and Ω is the atomic volume). Thus, the fragment including the C5═C6 bonds plays an important role both in the reactivity and bioactivity of the hydropyrimidines. In (1), a significant difference in both the charges and energies of the C6 and C5 atoms belonging to the conjugated C6═C5—C5′ = O1 moiety is observed (Table 4). This difference in charge exceeds that of ~ 0.1 e found for 5-acyl-substituted hydropyrimidines (Bartashevich *et al.*, 2006) and thus we suggest that (1) will provide stronger regiospecificity for addition reactions when compared with 5-acylhydropyrimidines.

We note that the molecular electronic energy that is obtained by summing the atomic energy contributions is in good quantitative agreement with the direct wavefunction calculation (Table 4). However, it is not accurate enough to estimate the energy of intermolecular interactions in the crystal.

3.4. Hydrogen bonds

The geometrical and topological parameters of the hydrogen bonds in (1) are given in Table 3. In agreement with the Koch & Popelier (1995) criteria of hydrogen-bond formation, the volumes of the H1, H3 and H62′ atoms involved in hydrogen bonds are decreased in the crystal compared with the free molecule. At the same time, the H62′ atom as well as the other atoms of the methyl group at position 6 are only slightly depopulated, and their energies in the crystal are more negative than those in the free molecule. In contrast, the H1 and H3 atoms, also involved in hydrogen bonds, behave exactly in agreement with the Koch & Popelier (1995) prediction. The facts given above are probably related to the non-linear geometry of the hydrogen bonds in (1), the most non-linear C6′—H62′···O1$^{\mathrm{i}}$ bond exhibiting the most prominent deviation from the Koch & Popelier (1995) criteria. All the hydrogen bonds are weak; however, the nonlinearity mentioned above makes an assessment of their strength using the bond CP characteristics doubtful.

3.5. Bond orders

We have also attempted to connect both bond and atomic features of the electron distribution with the traditional orbital-based descriptor of atomic interactions. The approach of Cioslowski & Mixon (1991) for the calculation of the covalent bond order, n_{CM}, provides such an opportunity. These workers suggested calculating the covalent bond order as follows. First, the elements of the atomic orbital matrix are computed by integrating the orbital products over zero-flux atomic basins, Ω_i. Then, unitary transformation among the occupied spin orbitals maximizes the number of electrons associated with a given atom and the covalent $A—B$ bond order is calculated with the use of the localized orbitals $\chi_i(\mathbf{r})$ as

$$n_{\mathrm{CM},AB} = 2\sum_i \int_{\Omega_A} \chi_i^*(\mathbf{r})\chi_i(\mathbf{r})\mathrm{d}V \int_{\Omega_B} \chi_i^*(\mathbf{r})\chi_i(\mathbf{r})\mathrm{d}V.$$

Howard & Lamarche (2003) have found that n_{CM} can be well approximated by the expression

$$n_{\mathrm{topo}} = a + b\lambda_3 + c(\lambda_1 + \lambda_2) + d\rho_b,$$

where λ_i are the electron-density curvatures and ρ_b is the ED at the bond CP, respectively. This expression, which combines the bond and atomic topological characteristics with a localized-orbital bonding description, was recognized as being suitable for both single and multiple bonds (Howard & Lamarche, 2003). It is important to stress that n_{topo} can be directly estimated using the topological features of the experimentally derived ED.

We have applied this approach to quantify the intramolecular bonds in (1). For the S—C, C—C and C—N bonds, the a, b, c and d coefficients recommended by Howard & Lamarche (2003) were used. For C—O, N—H and C—H bonds, we derived the corresponding coefficients by fitting n_{topo} to the n_{CM} for 46 C—O covalent bonds and for 49 X—H (X = C, N) covalent bonds in various organic molecules. It was found that the same coefficient set, $a = -0.072$, $b = 0.352$ $c = 0.114$, $d = 5.050$, provides a good fit for both N—H and C—H bonds (the correlation coefficient $R = 0.98$, the Fisher test $F = 864.6$, and the r.m.s. deviation = 0.037). For the C—O bond we have found the following coefficients: $a = -0.427$, $b = 0.280$, $c = -0.240$, $d = 6.464$ ($R = 0.92$; $F = 81.8$; r.m.s. = 0.08). The bond orders, n_{topo}, derived from the experimental and theoretical

Table 6
Cioslowski–Mixon bond-order parameters, n_{CM}, computed from the molecular wavefunctions for (1) and topological bond order, n_{topo}, computed from the multipole-modeled topological characteristics of the experimental and theoretical (*CRYSTAL*98) electron densities.

Pauling's bond orders are also listed. See text for details.

Bond	R (Å)	n_{CM}	$n_{topo,\ theor.}$ (mol)	$n_{topo,\ theor.}$ (cryst)	$n_{topo,\ exp}$	$n_{Pauling}$
S–C2	1.69	1.52	1.80	1.54	1.47	1.62
O1–C5′	1.23	1.26	1.24	1.41	1.64	1.37
O2–C5′	1.33	0.87	0.97	1.11	1.14	1.05
O2–C7	1.45	0.82	0.74	0.67	0.73	0.79
N1–C2	1.37	1.02	1.19	1.23	1.28	1.24
N1–C6	1.39	1.17	1.14	1.19	1.23	1.15
N1–H1	1.01	0.77	0.84	1.01	1.00	–
N3–C2	1.33	1.14	1.31	1.33	1.40	1.42
N3–C4	1.47	0.90	0.95	1.02	1.02	0.90
N3–H3	1.01	0.79	0.85	1.02	1.05	–
C4–C4′	1.53	0.95	0.92	0.62	0.64	0.96
C4–C5	1.52	0.97	1.07	0.73	0.71	1.02
C4–H4	1.09	0.90	0.91	1.02	1.00	–
C4′–H41′	1.06	0.95	0.92	1.06	0.96	–
C4′–H42′	1.06	0.96	0.92	1.06	0.96	–
C4′–H43′	1.06	0.96	0.92	1.05	0.96	–
C5–C5′	1.47	1.02	1.20	1.03	0.95	1.21
C5–C6	1.36	1.74	1.73	1.59	1.43	1.73
C6–C6′	1.50	1.18	1.06	0.78	0.78	1.08
C6′–H61′	1.06	0.95	0.92	1.05	1.09	–
C6′–H62′	1.06	0.96	0.92	1.06	1.08	–
C6′–H63′	1.06	0.96	0.92	1.06	1.05	–
C7–C8	1.51	0.98	1.02	0.72	0.76	1.04
C7–H71	1.09	0.91	0.89	1.01	1.01	–
C7–H72	1.09	0.91	0.89	1.01	0.99	–
C8–H81	1.06	0.96	0.92	1.06	1.03	–
C8–H82	1.06	0.96	0.92	1.06	0.99	–
C8–H83	1.06	0.96	0.92	1.05	0.98	–

electron densities are given in Table 6. The sum of the bond-order values over the atom can be regarded as the atomic valence index, V_A; corresponding experimental and theoretical values are listed in Table 7.

The r.m.s. deviation of the experimental and calculated values of the covalent bond orders averaged over all the intramolecular bonds in (1) is 0.173 (16.6%); the corresponding value for the atomic valence indices is 0.285 (13.7%).

Pauling's (1960) bond order $n_P = \exp[(r_0 - R)/a]$, where R is the bond length, was also computed for selected bonds (Table 6) using the values of r_0 and a given by Howard & Lamarche (2003). There is good agreement with the oversimplified classical view of the covalent bond order, as already noted by Macchi *et al.* (1998) and Stash *et al.* (2005). At the same time, Cioslowski & Mixon's index n_{CM} and the corresponding topological bond order, n_{topo}, more adequately mirror the actual electron-density distribution, although Angyan *et al.* (1994) noted that n_{CM} mainly reflects the covalent part of the bond and, therefore, shows magnitudes lower than the formal values. In spite of that, the n_{topo} index proves to be a suitable descriptor of the covalent bond order, keeping in mind the model dependence of the topological features of the experimental electron density discussed above.

The atomic valence index, V_A, describes atomic valence saturation: unsaturated atoms with a low value of V_A are able to participate in additional interactions, *i.e.* they are more reactive. From this point of view, the most reactive among the C atoms is C5′; the most reactive amongst the H atoms are the amino H1 and H3 atoms; their involvement in hydrogen bonding in the crystal diminish their reactivity noticeably. The V_A indices of the N1 and N3 atoms are comparable. The O1 atom also has an unsaturated valence; this correlates well with its ability to participate in the 'subsidiary' O1–C4′ bonding interaction found by Rykounov *et al.* (2005) for some conformers of (1), and to form the bifurcated hydrogen bonds in the crystal.

The most conspicuous discrepancy in the experimental and calculated atomic valence index is observed for the thiourea fragment of the heterocycle and the H atoms of the methyl group at the C6′ position. We stress that these parts of (1) are involved in the formation of the hydrogen-bond network in the crystal.

We can also note that proton donors, such as the N1 and N3 atoms, exhibit reduced calculated bond orders and atomic valence indices, respectively, compared with the experimental ones. On the contrary, proton acceptors such as the S and O1 atoms have larger calculated bond orders than the experimental values. Thus, the discrepancy of the covalent bond orders in the experimental data can reflect the influence of the intermolecular bond. In addition, the redistribution of electrons due to the intramolecular C6′–O2 bonding contact reduces the n_{topo} value of the C6–C6′ bond in the experimental case.

4. Summary

Our study shows that local values of the electron density at the bond CPs derived by different methods are in reasonable pairwise agreement. We confirmed the earlier results dealing with the elucidation of the origin of the discrepancy of the Laplacian of the electron density computed from wavefunctions and that derived from experimental or theoretical structure factors in terms of the multipole model. It is clearer now that an important (but not comprehensive) source of disagreement between DFT-formulae-based and wavefunction-based local-energy characteristics for shared interactions results from the model bias of the longitudinal ED curvature, λ_3, which is related to the deficiency of the ED description in the current multipole models. This deficiency runs through all the existing QTAMC bonding descriptors which contain the Laplacian term, including the topological bond orders and atomic valence indices derived in this work from the experimental ED for the first time. At the same time, the integrated atomic characteristics suffer much less from the above-

Table 7
Atomic valence indexes computed at the experimental geometry.

$V_{topo,exp}$ are experimental values, $V_{topo,theor}$(cryst) were obtained from the multipole-model parameters deduced using *CRYSTAL*98 structure factors, $V_{topo,theor}$(mol) were obtained using topological characteristics derived from the molecular DFT B3LYP/6-311G(d,p) wavefunctions and V_{CM} are quantities obtained from Cioslowski & Mixon (1991) bond orders.

	V_A			
Atom	$V_{topo,exp}$	$V_{topo,theor}$ (cryst)	$V_{topo,theor}$ (mol)	V_{CM}
S	1.47	1.54	1.80	1.52
O1	1.64	1.41	1.24	1.26
O2	1.87	1.78	1.71	1.69
N1	3.51	3.43	3.16	2.96
N3	3.46	3.37	3.11	2.83
C2	4.14	4.10	4.30	3.68
C4	3.36	3.39	3.85	3.71
C4′	3.51	3.79	3.69	3.82
C5	3.09	3.35	3.99	3.73
C5′	3.73	3.54	3.40	3.15
C6	3.43	3.57	3.92	4.09
C6′	4.00	3.94	3.82	4.04
C7	3.48	3.40	3.55	3.63
C8	3.75	3.89	3.79	3.87
H1	1.00	1.01	0.84	0.77
H3	1.05	1.02	0.92	0.79
H4	1.00	1.02	0.91	0.90
H41′	0.96	1.06	0.92	0.95
H42′	0.96	1.06	0.92	0.96
H43′	0.96	1.05	0.92	0.96
H61′	1.09	1.05	0.92	0.95
H62′	1.08	1.06	0.92	0.96
H63′	1.05	1.06	0.92	0.96
H71	1.01	1.01	0.89	0.91
H72	0.99	1.01	0.89	0.91
H81	1.03	1.06	0.92	0.96
H82	0.99	1.06	0.92	0.96
H83	0.98	1.05	0.92	0.96

mentioned shortcoming. The QTAMC quantities derived from wavefunctions are nowadays the most suitable candidates for analysis of the transferability of atoms and atomic groups in similar compounds. The question of whether crystalline or single-molecule calculations should be employed for this purpose depends on the aim of each specific study.

This work was supported by the Russian Foundation for Basic Research (grant 04–03-33053) and the Russian Federal Agency for Education (Program 'Development of the Highest-School Scientific Potential, 2006–2008', Projects 2.1.1. 5051 and 2.1.1. 9693).

References

Abramov, Yu. A. (1997). *Acta Cryst.* A**53**, 264–272.
Angyan, J., Loos, M. & Mayer, I. (1994). *J. Phys. Chem.* **98**, 5244–5248.
Atwal, K. S., Swanson, B. N., Unger, S. E., Floyd, D. M., Moreland, S., Hedberg, A. & O'Reilly, B. C. (1991). *J. Med. Chem.* **34**, 806–811.
Bader, R. F. W. (1990). *Atoms in Molecules: A Quantum Theory. The International Series of Monographs of Chemistry*, edited by J. Halpen & M. L. H. Green. Oxford: Clarendon Press.
Bader, R. F. W. (2005). *Monatsh. Chem.* **136**, 819–854.
Bader, R. F. W. & Beddall, P. M. (1972). *J. Chem. Phys.* **56**, 3320–3329.
Bartashevich, E. V., Pereyaslavskaya, E. S., Grishina, M. A., Potemkin, V. A., Fedorova, O. V. & Rusinov, G. L. (2006). MedChemEurope, 21–22 February 2006, Prague. Book of Abstracts, pp. 125–126.
Bianchi, R., Gatti, C., Adovasio, V. & Nardelli, M. (1996). *Acta Cryst.* B**52**, 471–478.
Bianchi, R., Gervasio, G. & Marabellow, D. (2000). *Inorg. Chem.* **39**, 2360–2366.
Biegler-Konig, F. W., Bader, R. F. W. & Tang, T.-H. (1982). *J. Comput. Chem.* **3**, 317–352.
Biginelli, P. (1893). *Gazz. Chim. Ital.* **23**, 360–413.
Blessing, R. H. (1987). *Cryst. Rev.* **1**, 3–58.
Blessing, R. H. (1989). *J. Appl. Cryst.* **22**, 396–397.
Breneman, C. M. & Rhem, M. J. (1997). *Comput. Chem.* **18**, 182–197.
Chang, C. & Bader, R. F. W. (1992). *J. Phys. Chem.* **96**, 1654–1662.
Chandler, G. S. & Spackman, M. A. (1982). *Acta Cryst.* A**38**, 225–239.
Cioslowski, J. & Mixon, S. T. (1991). *J. Am. Chem. Soc.* **113**, 4142–4145.
Connolly, M. L. (1983). *J. Appl. Cryst.* **16**, 548–558.
Connolly, M. L. (1985). *J. Am. Chem. Soc.* **107**, 1118–1124.
Coppens, P., Abramov, Yu., Carducci, M., Korjov, B., Novozhilova, I., Alhambra, C. & Pressprich, M. R. (1999). *J. Am. Chem. Soc.* **121**, 2585–2593.
Coppens, P. & Volkov, A. (2004). *Acta Cryst.* A**60**, 357–364.
Cortes-Guzman, F. & Bader, R. F. W. (2004). *J. Phys. Org. Chem.* **17**, 95–99.
Cremer, D. & Kraka, E. (1984). *Croat. Chem. Acta*, **57**, 1259–1281.
Dittrich, B., Koritsanszky, T., Grosche, M., Scherer, W., Flaig, R., Wagner, A., Krane, H. G., Kessler, H., Riemer, C., Schreur, A. M. M. & Luger, P. (2002). *Acta Cryst.* B**58**, 721–727.
Dittrich, B., Scheins, S., Paulmann, C. & Luger, P. (2003). *J. Phys. Chem. A*, **107**, 7471–7474.
Espinosa, E., Alkorta, I., Elguero, J. & Molins, E. (2002). *J. Chem. Phys.* **117**, 5529–5542.
Espinosa, E., Lecomte, C., Molins, E., Veintemillas, S., Cousson, A. & Paulus, W. (1996). *Acta Cryst.* B**52**, 519–534.
Espinosa, E., Molins, E. & Lecomte, C. (1998). *Chem. Phys. Lett.* **285**, 170–173.
Fabian, W. M. F., Semones, M. A. & Kappe, C. O. (1998). *J. Mol. Struct. Theochem.* **432**, 219–228.
Farrugia, L. J., Mallinson, P. R. & Stewart, B. (2003). *Acta Cryst.* B**59**, 234–247.
Flaig, R., Koritsanszky, T., Dittrich, B., Wagner, A. & Luger, P. (2002). *J. Am. Chem. Soc.* **124**, 3407–3417.
Galvez, O., Gomez, O. & Pacios, L. F. (2001). *Chem. Phys. Lett.* **337**, 263–268.
Gatti, C. (2005). *Z. Kristallogr.* **220**, 399–457.
Granovsky, A. A. (2003). http://classic.chem.msu.su/gran/gamess/index.html.
Grover, G. J., Dzwonczyk, S., McMullen, D. M., Normandin, D. E., Parham, C. S., Sleph, P. G. & Moreland, S. (1995). *J. Cardiovasc. Pharmacol.* **26**, 289–294.
Gurskaya, G. V., Zavodnik, V. E. & Shutalev, A. D. (2003*a*). *Cryst. Rep.* **48**, 92–97.
Gurskaya, G. V., Zavodnik, V. E. & Shutalev, A. D. (2003*b*). *Cryst. Rep.* **48**, 416–421.
Haggarty, S. J., Mayer, T. U., Miyamoto, D. T., Fathi, R., King, R. W., Mitchison, T. J. & Schreiber, S. L. (2000). *Chem. Biol.* **7**, 275–286.
Hansen, N. K. & Coppens, P. (1978). *Acta Cryst.* A**34**, 909–921.
Henn, J., Ilge, D., Leusser, D., Stalke, D. & Engels, B. (2004). *J. Phys. Chem. A*, **108**, 9442–9452.
Hibbs, D. E., Overgaard, J., Howard, S. T. & Nguyen, T. H. (2005). *Org. Biomol. Chem.* **3**, 441–447.
Howard, S. T. & Lamarche, O. (2003). *J. Phys. Org. Chem.* **16**, 133–141.
Iversen, B. B., Larsen, F. K., Figgis, B. N. & Reynolds, P. A. (1997). *J. Chem. Soc. Dalton Trans.* pp. 2227–2240.
Jelsch, C., Teeter, M. M., Lamzin, V., Pichon-Pesme, V., Blessing, R. H. & Lecomte, C. (2000). *Proc. Natl. Acad. Sci. USA*, **97**, 3171–3176.

Kappe, C. O. (1993). *Tetrahedron*, **49**, 6937–6963.
Kappe, C. O. (2000*a*). *Acc. Chem. Res.* **33**, 879–888.
Kappe, C. O. (2000*b*). *Eur. J. Med. Chem. Chim. Theor.* **35**, 1043–1052.
Kappe, C. O., Fabian, W. M. F. & Semones, M. A. (1997). *Tetrahedron*, **53**, 2803–2816.
Kappe, C. O., Shishkin, O. V., Uray, G. & Verdino, P. (2000). *Tetrahedron*, **56**, 1859–1862.
Kirzhnits, D. A. (1957). *Sov. Phys. JETP*, **5**, 64–72.
Koch, U. & Popelier, P. L. A. (1995). *J. Phys. Chem.* **99**, 9747–9754.
Koritsanszky, T., Volkov, A. & Coppens, P. (2002). *Acta Cryst.* A**58**, 464–472.
Lecomte, C., Guillot, B., Jelsch, C. & Podjarny, A. (2005). *Int. J. Quant. Chem.* **101**, 624–634.
Lee, H., Lee, C. & Parr, R. G. (1991). *Phys. Rev. A*, **44**, 768–771.
Lobanov, N. N., Shchedrin, B. M. & Tsirelson, V. G. (1990). *Sov. Phys. Crystallogr.* **35**, 344–347.
Macchi, P. & Coppens, P. (2001). *Acta Cryst.* A**57**, 656–662.
Macchi, P., Proserpio, D. M. & Sironi A. (1998). *J. Am. Chem. Soc.* **120**, 1447–1455.
Macchi, P. & Sironi, A. (2003). *Coord. Chem. Rev*. **238–239**, 383–412.
Marabello, D., Bianchi, R., Gervasio, G. & Cargnoni, F. (2004). *Acta Cryst.* A**60**, 494–501.
Matta, C. F. & Bader, R. F. W. (2000). *Proteins Struct. Funct. Genet.* **40**, 310–329.
Matta, C. F. & Bader, R. F. W. (2002). *Proteins Struct. Funct. Genet.* **48**, 519–538.
Matta, C. F. & Bader, R. F. W. (2003). *Proteins Struct. Funct. Genet.* **52**, 360–399.
Nagarathnam, D. *et al.* (1999). *J. Med. Chem.* **42**, 4764–4777.
O'Brien, S. E. & Popelier, P. L. A. (1999). *Can. J. Chem.* **77**, 28–36.
O'Brien, S. E. & Popelier, P. L. A. (2001). *J. Chem. Inf. Comput. Sci.* **41**, 764–775.
Parini, E. V., Tsirelson, V. G. & Ozerov, R. P. (1985). *Sov. Phys. Crystallogr.* **30**, 497–502.
Pauling, L. (1960). *The Nature of the Chemical Bond*. Ithaca, NY: Cornell University Press.
Pichon-Pesme, V., Jelsch, C., Guillot, B. & Lecomte, C. (2004). *Acta Cryst.* A**60**, 204–208.
Pichon-Pesme, V., Lecomte, C. & Lachekar, H. (1995). *J. Phys. Chem.* **99**, 6242–6250.
Politzer, P. & Parr, R. G. (1974). *J. Chem. Phys.* **61**, 4258–4262.
Popelier, P. L. A. (1999). *J. Phys. Chem. A*, **103**, 2883–2890.
Popelier, P. L. A. & Aicken, F. M. (2003). *J. Am. Chem. Soc.* **125**, 1284–1292.
Popelier, P. L. A. & Bader, R. F. W. (1994). *J. Phys. Chem.* **98**, 4473–4481.
Protas, J. (1997). *MOLDOS*97/*MOLLY* MS DOS Updated Version. Private Communication.
Rovnyak, G. C., Kimball, S. D., Beyer, B., Cucinotta, G., DiMarco, J. D., Gougoutas, J., Hedberg, A., Malley, M., McCarthy, J. P., Zhang, R. & Moreland, S. (1995). *J. Med. Chem.* **38**, 119–129.
Rykounov, A., Potemkin, V., Stash, A. & Tsirelson, V. (2005). *Adv. Chem. Chem. Technol.* **19**, 87–91 (in Russian).
Saunders, V. R., Dovesi, R., Roetti, C., Causà, M., Harrison, N. M., Orlando, R. & Zicovich-Wilson, C. M. (1998). *CRYSTAL*98 User's Manual. University of Torino, Italy.
Schmidt, M. W., Baldridge, K. K., Boatz, J. A., Elbert, S. T., Gordon, M. S., Jensen, J. J., Koseki, S., Matsunaga, N., Nguyen, K. A., Su, S., Windus, T. L., Dupuis, M. & Montgomery, J. A. (1993). *J. Comput. Chem.* **14**, 1347–1363.
Sheldrick, G. M. (1997). *SHELXTL*, Version 5.1. University of Göttingen, Germany.
Shishkin, O. V., Solomovich, E. V., Vakula, V. M. & Yaremenko, F. G. (1997). *Russ. Chem. Bl.* **46**, 1838–1843.
Shutalev, A. D. & Kuksa, V. A. (1997). *Khim. Geterotsiclicheskich Soedin.* pp. 105–109 (in Russian).
Shutalev, A. D., Kishko, E. A., Sivova, N. V. & Kuznetsov, A. Yu. (1998). *Molecules*, **3**, 100–106.
Siemens (1996*a*). *SMART*5.054. Siemens Analytical X-ray Instruments Inc., Madison, Wisconsin, USA.
Siemens (1996*b*). *SAINT*. Siemens Analytical X-ray Instruments Inc., Madison, Wisconsin, USA.
Spackman, M. A., Byrom, P. G., Alfredsson, M. & Hermansson, K. (1999). *Acta Cryst.* A**55**, 30–47.
Stash, A. I. (2003). Proc. of the 28th ISTC Japan Workshop on Frontiers of X-ray Diffraction Technologies in Russia/CIS. Nagoya, pp. 147–153.
Stash, A. I., Tanaka, K., Shiozawa, K., Makino, H. & Tsirelson, V. G. (2005). *Acta Cryst.* B**61**, 418–428.
Stash, A. & Tsirelson, V. (2002). *J. Appl. Cryst.* **35**, 371–373.
Stash, A. I. & Tsirelson, V. G. (2005). *Cryst. Rep.* **50**, 177–184.
Tal, Y. & Bader, R. F. W. (1978). *Int. J. Quantum Chem. Symp.* **12**, 153–168.
Tsirelson, V. (1999). *Acta Cryst.* A**55**, Abstract M13-OF-003, S207.
Tsirelson, V. G. (2002). *Acta Cryst.* B**58**, 632–639.
Tsirelson, V. G. (2003). 3rd Europian Charge Density Meeting and European Science Foundation Exploratory Workshop (ECDM-III). Sandbjerg Estate, Denmark, 2003, p. O7.
Vries, R. de, Feil, D. & Tsirelson, V. G. (2000). *Acta Cryst.* B**56**, 118–123.
Volkov, A., Abramov, Y., Coppens, P. & Gatti, C. (2000). *Acta Cryst.* A**56**, 332–339.
Volkov, A. & Coppens, P. (2001). *Acta Cryst.* A**57**, 395–405.
Volkov, A., Koritsanszky, T., Li, X. & Coppens, P. (2004). *Acta Cryst.* A**60**, 638–639.
Volkov, A., Li, X., Koritsanszky, T. & Coppens, P. (2004). *J. Phys. Chem. A*, **108**, 4283–4300.
Whitehead, C. E., Breneman, C. M., Sukumar, N. & Ryan, M. D. (2003). *J. Comput. Chem.* **24**, 512–529.
Uray, G., Verdino, P., Belaj, F., Kappe, C. O. & Fabian, W. M. F. (2001). *J. Org. Chem.* **66**, 6685–6694.
Zavodnik, V. E., Shutalev, A. D., Gurskaya, G. V., Stash, A. I. & Tsirelson, V. G. (2005). *Acta Cryst.* E**61**, o468–o470.
Zhurova, E. A., Tsirelson, V. G., Stash, A. I., Yakovlev, M. V. & Pinkerton, A. A. (2004). *J. Phys. Chem. B*, **108**, 20173–20179.